Full Speed Range Sensorless IPMSM Drive Enhanced with Online Parameter Identification

Aravinda Perera
Department of Electric Power Engineering
Norwegian University of Science and Technology
Trondheim, Norway
aravinda.perera@ntnu.no

Roy Nilsen
Department of Electric Power Engineering
Norwegian University of Science and Technology
Trondheim, Norway
roy.nilsen@ntnu.no

***Abstract*— This paper aims to combine the state-of-the-art parameter-adaptation and state-estimation techniques to realize an adaptive and sensorless interior permanent magnet synchronous machine (IPMSM) drive that offers robust performance across the full speed range even in the presence of temperature-variations. Recursive prediction error based Online Parameter Estimator (OPE) accompanied by a gain-scheduler adapts temperature-sensitive motor parameters, i.e. the stator resistance (R_s) and permanent magnet flux linkage (Ψ_m) in the lower and higher speed regions respectively. The Active Flux Observer (AFO) and the Pulsating sqUare-wave Voltage Injection (PUVI) based saliency tracking method are adopted to estimate the rotor position in the higher and lower speed regions respectively. The OPE augments the performance of the AFO across a large part of the speed-range and the use of PUVI-based technique eliminates the potential precision-compromise of the estimated position due to the gain-scheduler in the low-speed region. Zynq System on Chip (SoC) based Embedded Real-Time Simulator (ERTS) is used to demonstrate the concepts, in which the drive control and estimation algorithms are programmed in its processor system and the drive hardware is modeled in its Field-Programmable Gate Array (FPGA).**

***Keywords*— Adaptive control, high frequency signal injection, observer, parameter estimation, sensor-less, system on chip, variable speed drive**

I. INTRODUCTION

Position-sensorless IPMSM drives are becoming the state-of-the-art in safety-critical traction and automation applications due to their superior efficiency, power density, ease of cooling, design capability for fault-tolerance, good control dynamics in a wide torque-speed range and enhanced reliability [1], [2].

In the high performance industrial drives, the sensorless control is realized by combining a fundamental excitation (FE)-based method in the mid and high speeds and a saliency tracking method in the very low speeds down to zero, in order to extract their optimal performances in different speed regions. Extended electromotive force (EEMF), Luenberger and sliding-mode observer types, Model Reference Adaptive Systems (MRAS) are among the common candidates for FE-based position-estimations. However, due to their increasing R_s-dependency and gradual disappearance of the FE signal when the rotor approaches standstill, alternative methods have been developed to estimate the rotor position, particularly for the applications that demand persistent low-speed operation. High frequency signal injection (HFSI) based method is among the promising alternatives which, in general, aim to track the magnetic saliency of the rotor. INFORM method or its improvements [3], [4] or Rotating Sinusoidal Voltage Injection (RSVI) method [5] or Pulsating Sinusoidal Voltage Injection (PSVI) [6] have been reported over the last decades, yet, they display either or a combination of drawbacks as such as discontinuous tracking, restrictions in the controller bandwidth, acoustic noise or considerable estimation error. PUVI method proposed in [7] and its improvements [8], [9] eliminate the requirement of a low-pass-filter (LPF) in the controllers, thus enhances the controller bandwidth and estimation precision significantly.

Irrespective of the position estimation method, the accurate knowledge of IPMSM electric parameters, i.e., the Ψ_m, R_s , d- and q- axis inductances L_d and L_q are essential to ensure precise and adaptive torque/speed control, condition monitoring, fault diagnosis and self-commissioning of electric drives [10]. A deviation of L_d and L_q from their datasheet values can be triggered by the magnetic saturation: a phenomenon and its effects which can be fairly identified using an offline identification method. Contrastingly, Ψ_m, R_s -deviations can be caused by the operating temperature which can vary due to unforeseen circumstances in certain applications, thus a recursive identification scheme for these parameters can become essential for precise torque/speed control. Online adaptation of temperature-sensitive parameters, on the other hand, is proven to enhance the torque/speed control at higher speeds and position estimation at low speeds [11], [12] when coupled with FE-based schemes. Due to the inherent coupling of Ψ_m and R_s and the rank-deficiency problem [10], gain-scheduling schemes have been utilized [11], [13], [14] to adapt only Ψ_m beyond very low speeds and only R_s around zero speed. Such scheduling however, can unduly adapt R_s in its adaptation-region due to potential Ψ_m-estimate errors, consequently the position-estimation precision is hampered [11].

Literature on the full speed range sensorless control assisted with online parameter estimation for AC machines has been scarce particularly, with the state-of-the-art methods. Ref [13], [15], and [16] discuss such complete control schemes, although, they adopt RSVI which bears inherent drawbacks as noted before. In [17] and [18], modern sensorless control methods are combined to cover the full-speed range, however, lacks online parameter adaptation.

In this letter, the authors aim to combine the Active Flux Observer (AFO) [19] and PUVI method [8] to achieve full speed range sensorless control including zero speed. The AFO is assisted by online adaptation of Ψ_m and R_s using prediction error gradients and stochastic gradient algorithm [14] in order to incorporate adaptive control in the drive. The drive concepts are validated using an embedded real-time simulator [20] in which the ARM processors contain the drive software and its FPGA section contains emulation models of IPMSM-drive.

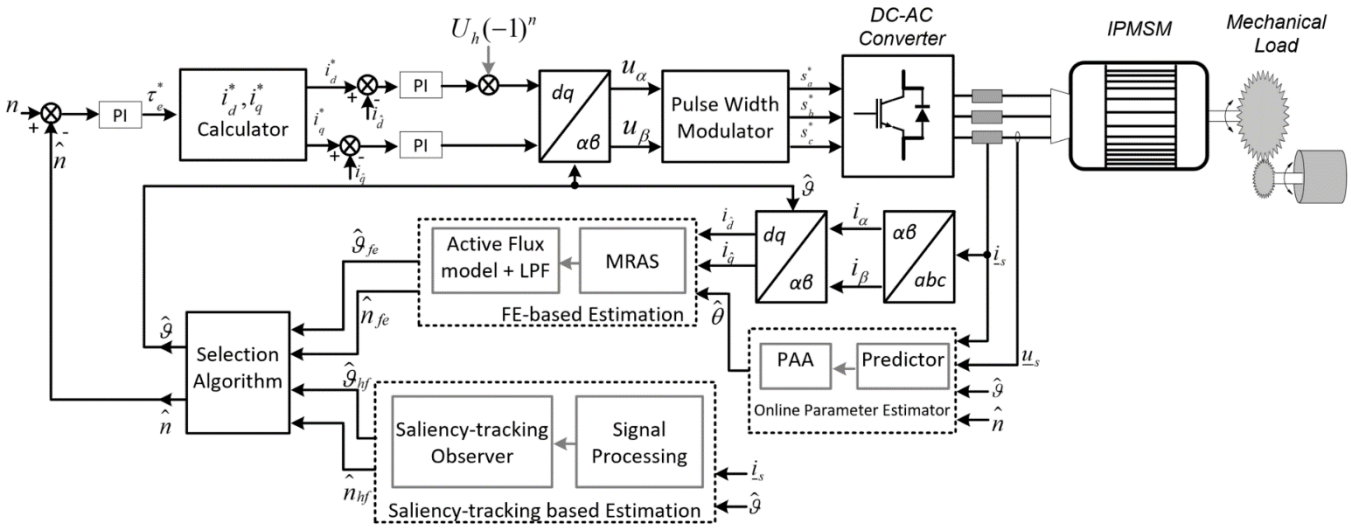

Fig. 1. Full speed range sensorless control scheme enhanced with online parameter identification of temperature-sensitive parameters

II. Sensorless and Adaptive IPMSM Drive

A. IPMSM Dynamic Model

The mathematical model of the electrical part of the machine is in the rotor co-ordinates, when given in the per-unit (pu) system:

$$\underline{u}_s^r = r_s \cdot \underline{i}_s^r + \frac{1}{\omega_n}\frac{d\underline{\psi}_s^r}{dt} + \mathbf{j}\cdot f_k \cdot \underline{\psi}_s^r, \quad \underline{\psi}_s^r = \mathbf{x}_s^r \cdot \underline{i}_s^r + \underline{\psi}_m^r \tag{1}$$

$$\underline{i}_s^r = [\,i_d \quad i_q\,]^T \quad \underline{\hat{\psi}}_m^r = [\hat{\psi}_m \quad 0]^T \quad \mathbf{x}_s^r = \begin{bmatrix} x_d & 0 \\ 0 & x_q \end{bmatrix} \quad \mathbf{j} = \begin{bmatrix} 0 & -1 \\ 1 & 0 \end{bmatrix}$$

Here, ω_n is the nominal rotational frequency. ϑ is the electrical angle of the mechanical position $p*\vartheta_{mech}$, where p is the number of pole pairs. Electrical speed in pu is denoted by n. The superscript and subscript denote the reference frame and the location of the quantity (s-stator, r-rotor, m-magnet) respectively.

B. Position Estimation Model at Medium and High Speeds

The position estimation adopts the AFO presented in [19]. Accordingly, a quantity called 'active flux' is defined as follows.

$$\underline{\hat{\psi}}_T^s = \omega_n \cdot \int (\underline{u}_s^s - \hat{r}_s \underline{i}_s^s + \underline{u}_{comp}^s)\cdot dt - \hat{x}_q \cdot \underline{i}_s^s = \underline{\hat{\psi}}_{s,u}^s - \hat{x}_q \cdot \underline{i}_s^s \tag{2}$$

Here, $\underline{\psi}_T$ is the active flux component. In this observer structure, the current model and voltage model are employed as the reference and adaptive model respectively. Thus, the reference model and adaptive model are given in (3) and (4).

$$\underline{\hat{\psi}}_{s,i}^r = \mathbf{x}_s^r \cdot \underline{i}_s^r + \underline{\psi}_m^r \tag{3}$$

$$\underline{\hat{\psi}}_{s,u}^s = \omega_n \cdot \int (\underline{u}_s^s - \hat{r}_s \cdot \underline{i}_s^s + \underline{u}_{comp}^s)\cdot dt \tag{4}$$

From which, the error, $\underline{\varepsilon}_{s,o}$ is calculated and attempted to eliminate with the aid of a proportional-integral (PI) compensator.

$$\underline{\varepsilon}_{s,o} = \underline{\hat{\psi}}_{s,i}^s - \underline{\hat{\psi}}_{s,u}^s \tag{5}$$

The integrator offset, parametric discrepancies, measurement errors, the dead-times in the Pulse Width Modulator (PWM)-inverter device switching and other nonlinearities of the IPMSM drive generates nonzero $\underline{\varepsilon}_{s,o}$. A proportional-integral (PI) controller can be used to drive the $\underline{\varepsilon}_{s,o}$ to zero. PI-tuning method is discussed in [16]. Therein, the AFO-based speed and position can be calculated using the following expressions.

$$\hat{\vartheta}_{fe} = \operatorname{atan2}\left(\frac{\hat{\psi}_{T,\beta}^s[k]}{\hat{\psi}_{T,\alpha}^s[k]}\right)$$

$$\hat{n}_{fe} = \frac{\hat{\psi}_{T,\alpha}^s[k-1]\cdot\hat{\psi}_{T,\beta}^s[k] - \hat{\psi}_{T,\beta}^s[k-1]\cdot\hat{\psi}_{T,\alpha}^s[k]}{T_{samp}\cdot\left(\left(\hat{\psi}_{T,\alpha}^s[k]\right)^2 + \left(\hat{\psi}_{T,\beta}^s[k]\right)^2\right)} \tag{6}$$

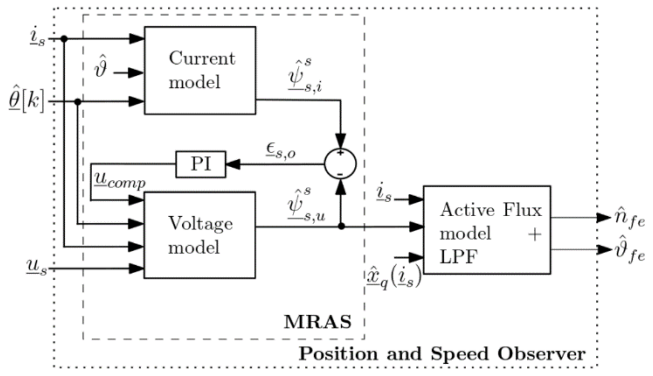

Fig. 2. Block diagram of Active Flux Observer

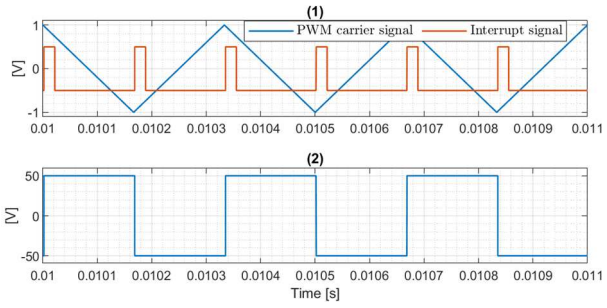

Fig. 3. (1) Double-update PWM signal and interrupt signal (2) injected square-wave signal on the d-axis

C. Position Estimation Model at Very Low Speed and Standstill

Square-wave voltage injection on the d-axis as illustrated in the Fig. 1, at the PWM switching frequency [8], is employed to estimate the rotor position at very low speeds including standstill. Fig. 3 shows the double-update PWM, the interrupt signal and the square-wave voltage carrier signal. The injected voltage is expressed as follows, where u_h and k are amplitude and injected voltage in per-unit:

$$\begin{bmatrix} u_{\hat{d}h} \\ u_{\hat{q}h} \end{bmatrix} = \begin{bmatrix} u_h(-1)^k \\ 0 \end{bmatrix} \tag{7}$$

The notations $\hat{d}, \hat{q}$ indicate the estimated rotor reference frame. Fig. 4 shows the relation between the reference frames. In [21], it is discussed how the q-axis high frequency current response is modulated with the rotor-position error information. Accordingly, the high frequency current responses can be expressed as follows.

$$\begin{bmatrix} \delta i_{\hat{d}h} \\ \delta i_{\hat{q}h} \end{bmatrix} = \frac{u_{\hat{d}h} \cdot \omega_n \cdot T_{samp}}{(\Delta x^2 - \Sigma x^2)} \cdot \begin{bmatrix} \Sigma x - \Delta x \cos(2\tilde{\vartheta}) \\ \Delta x \sin(2\tilde{\vartheta}) \end{bmatrix}$$
$$\delta i_{\hat{d}h} = i_{\hat{d}h}[k] - i_{\hat{d}h}[k-1];\ \delta i_{\hat{q}h} = i_{\hat{q}h}[k] - i_{\hat{q}h}[k-1] \tag{8}$$
$$\Sigma x = 0.5 \cdot (x_d + x_q);\ \Delta x = 0.5 \cdot (x_d - x_q)$$

$\tilde{\vartheta}$ is the rotor position estimation error as illustrated in the Fig. 4. In the given HFSI scheme, since the injection frequency is relatively much higher than the FE-frequency, the current response to the FE can be assumed almost constant in one sampling period [21], therefore the sampling current can be approximated to that of the high frequency current response:

$$\delta i_{\hat{q}h} \approx \delta i_{\hat{q}} = i_{\hat{q}}[k] - i_{\hat{q}}[k-1] \tag{9}$$

Thus, it can be deduced that the position estimation error is as follows, in per-unit:

$$\tilde{\vartheta} \approx \frac{x_d \cdot x_q}{(x_q - x_d) \cdot u_{\hat{d}h}[k] \cdot \omega_n \cdot T_{samp}} \cdot \delta i_{\hat{q}} = K_{hf} \cdot \delta i_{\hat{q}} \tag{10}$$

The position estimation error can be extracted either with use of (10) or alternative methods as such as orthogonal measurement axes [8]. Subsequently, the rotor position can be obtained using the estimation error with use of a saliency tracking observer in the form of a second-order phase-locked-loop (PLL) or a more advanced observer known as extended state observer [22]. In this paper, the authors use a PLL to estimate the rotor position when PUVI-technique is adopted in the low speed region. Fig. 5 illustrates the corresponding scheme. It is worth noting that the PUVI-based position estimation coupled with a PLL does not rely on the electrical parameters of the machine, which makes it insensitive to parameter variations.

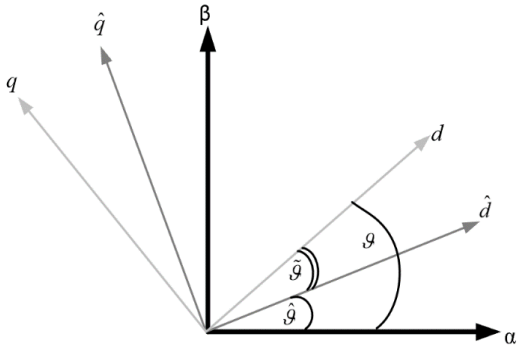

Fig. 4. Illustration of reference frames in the control scheme and their relative positioning

D. Online Parameter Estimation Model

The online parameter estimation (OPE) model proposed in [14] is adopted in this letter which is placed in context in the Fig. 1. The inherent sensitivities of this model to the model-parameter discrepancies will be capitalized in the proposed parameter adaptation algorithm (PAA). Full-order model ($\mathcal{M}_{u\vartheta}$), is used with stator currents chosen as state variables. The rotor-oriented model is chosen for current prediction in the predictor.

$$\underline{u}_s^r = \hat{r}_s \cdot \underline{\hat{i}}_s^r + \frac{\mathbf{x}_s^r}{\omega_n} \cdot \frac{d\underline{\hat{i}}_s^r}{dt} + \mathbf{j} \cdot n \cdot \hat{\mathbf{x}}_s^r \cdot \underline{\hat{i}}_s^r + \mathbf{j} \cdot n \cdot \underline{\hat{\psi}}_m^r \tag{11}$$
$$\hat{\underline{\theta}} = \begin{bmatrix} \hat{\psi}_m & \hat{r}_s \end{bmatrix}^T \quad \underline{i}_s^r = \mathbf{T}_{ss}^r(\vartheta) \cdot \underline{i}_s^s \qquad \underline{u}_s^r = \mathbf{T}_{ss}^r(\vartheta) \cdot \underline{u}_s^s$$

Here, from the estimated parameter matrix, $\hat{\underline{\theta}}$, $\hat{x}_d, \hat{x}_q$ are omitted to curtail the discussion only to scope of interest. $\mathcal{M}_{u\vartheta}$ is a second order system and the eigenvalues of this model are speed dependent. The system matrix **A** of the system can be expressed as:

$$\lambda \cdot I_2 - \mathbf{A} = \begin{bmatrix} \lambda + \frac{\omega_n \cdot \hat{r}_s}{\hat{x}_d} & -\frac{\omega_n \cdot n \cdot \hat{x}_q}{\hat{x}_d} \\ \frac{\omega_n \cdot n \cdot \hat{x}_d}{\hat{x}_q} & \lambda + \frac{\omega_n \cdot \hat{r}_s}{\hat{x}_q} \end{bmatrix} \quad T_d = \frac{x_d}{r_s \cdot \omega_n}, T_q = \frac{x_q}{r_s \cdot \omega_n} \tag{12}$$

The eigenvalues become:

$$\lambda_{1,2} = -\frac{1}{2} \cdot \left(\frac{1}{\hat{T}_d} + \frac{1}{\hat{T}_q} \right) \pm \sqrt{\left(\frac{1}{2} \cdot \left(\frac{1}{\hat{T}_d} + \frac{1}{\hat{T}_q} \right) \right)^2 - \left(\frac{1}{\hat{T}_d \cdot \hat{T}_q} + (\omega_n \cdot n)^2 \right)} \tag{13}$$

E. Decoupling Technique

Despite ψ_m and r_s are identifiable simultaneously under certain conditions, these parameters are inherently coupled, and their coupling and points of natural decoupling are discussed in [10]. The effect of coupling is analyzed in [11] where it was found out that due to ψ_m-estimate errors ($\delta\psi_m$), r_s-estimate gets heavily penalized because $r_s << \psi_m$ in per-unit. Due to this large asymmetricity in magnitudes, the penalty on ψ_m-estimate due to r_s-estimate errors (δr_s) is not considerable unless n is very small. The proposed gain-scheduler in [11] circumvents the coupling issue with respect to ψ_m, but not w.r.t r_s, thus if ψ_m is erroneous in the r_s-adaptation zone, r_s gets unfairly compensated.

The effect of such erroneous r_s can be evident in the torque-speed control of a sensorless IPMSM drive in [11]. Such performance degradation is expected to be eliminated

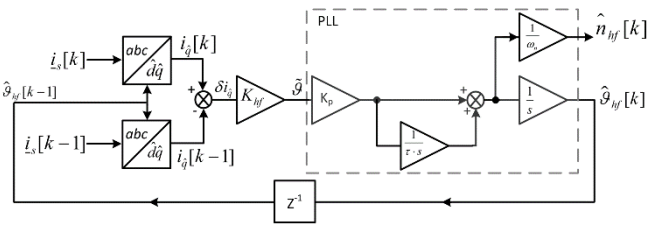

Fig. 5. Demodulation and saliency tracking-PLL for PUVI method

in this research work with use of a parameter-independent sensorless control scheme like the PUVI-based rotor position tracking in the r_s-adaptation speed zone.

III. Parameter Adaptation Algorithm

A. Recursive Prediction Error Method

A numerical estimation approach known as Recursive Prediction Error Method (RPEM) is adopted as the parameter adaptation algorithm in this scope to recursively track ψ_m and r_s. RPEM in discrete form based on the Forward Euler Method, becomes, where D_M is the defined parameter space:

$$\underline{\hat{\theta}}[k]=\left[\underline{\hat{\theta}}[k-1]+\mathbf{L}[k]\cdot\underline{\varepsilon}_s^r[k]\right]_{D_M};D_M=\begin{Bmatrix}\psi_{m,\min}\le\hat{\psi}_m\le\psi_{m,\max}\\ r_{s,\min}\le\hat{r}_s\le r_{s,\max}\end{Bmatrix} \quad (14)$$

$\boldsymbol{L}$[k], the gain-matrix and $\underline{\varepsilon}^r_s$ in steady state, in component form, ε_d, ε_q are given in (15) and (16) respectively.

$$\mathbf{L}[k]=\begin{bmatrix}L_{11}[k] & L_{12}[k]\\ L_{21}[k] & L_{22}[k]\end{bmatrix},\quad \begin{matrix}L_{11},L_{12}=\text{gains of }\hat{\psi}_m\\ L_{21},L_{22}=\text{gains of }\hat{r}_s\end{matrix} \quad (15)$$

$$\varepsilon_d=-\frac{n^2\cdot\hat{x}_q}{\hat{r}_s^2+n^2\cdot\hat{x}_q\cdot\hat{x}_d}\cdot\delta\psi_m-\left[\frac{\hat{r}_s}{\hat{r}_s^2+n^2\cdot\hat{x}_q\cdot\hat{x}_d}\cdot i_d+\frac{n\cdot\hat{x}_q}{\hat{r}_s^2+n^2\cdot\hat{x}_q\cdot\hat{x}_d}\cdot i_q\right]\cdot\delta r$$

$$\varepsilon_q=-\frac{n\cdot\hat{r}_s}{\hat{r}_s^2+n^2\cdot\hat{x}_q\cdot\hat{x}_d}\cdot\delta\psi_m-\left[\frac{\hat{r}_s}{\hat{r}_s^2+n^2\cdot\hat{x}_q\cdot\hat{x}_d}\cdot i_q-\frac{n\cdot\hat{x}_d}{\hat{r}_s^2+n^2\cdot\hat{x}_q\cdot\hat{x}_d}\cdot i_d\right]\cdot\delta r \quad (16)$$

$$\delta\psi_m=\psi_m-\hat{\psi}_m,\ \delta r_s=r_s-\hat{r}$$

B. Stochastic Gradient Algorithm

To rapidly identify the gain matrix $\boldsymbol{L}$[k] for accurate identification of $\underline{\hat{\theta}}$ in D_M, a sub-algorithm known as stochastic gradient algorithm (SGA) is applied, which is:

$$\mathbf{L}[k]=\gamma[k]\cdot\frac{\boldsymbol{\Psi}^T[k]}{r[k]}$$

$$\gamma[k]=\gamma_0=\frac{T_{samp}}{T_0} \quad (17)$$

$$\boldsymbol{\Psi}^T=\left[\left(\frac{d\hat{\underline{i}}_s^r[k,\hat{\psi}_m]}{d\hat{\psi}_m}\right)_{steady-state}\quad\left(\frac{d\hat{\underline{i}}_s^r[k,\hat{r}_s]}{d\hat{r}_s}\right)_{dynamic-state}\right]$$

$$r[k]=r[k-1]+\gamma[k]\cdot\left\{tr\left[\boldsymbol{\Psi}[k]\cdot\boldsymbol{\Psi}^T[k]\right]-r[k-1]\right\}$$

Here, the sensitivity of the prediction error against the estimated parameter, known as prediction-error gradient, (denoted by $\boldsymbol{\Psi}^T$) is the heart of the parameter adaptation algorithm. It's influence and behavior in the IPMSM-context is analyzed in [10], [14] and [23].

IV. Real-Time Simulation Results & Discussion

Xilinx Zynq SoC based Embedded Real-Time Simulator has been used to validate the proposed control scheme. The power hardware components of the IPMSM drive, i.e., 3-phase IPMSM, 2-level PWM-inverter and the mechanical load models are programmed in the FPGA fabric of the SoC to achieve real-time emulation. The field-oriented control to achieve Maximum Torque Per Ampere (MTPA) strategy, field-weakening control, state- and parameter- estimation algorithms and likewise processes that do not demand extremely high processing speeds are programmed in the on-chip processor using C++ programming language. The routines programmed in the processor are intended to drive either the on-chip emulation models or the physical hardware. Digital to analog (DAC) feature of the digital control platform can be used to capture the high bandwidth data real-time with the help of an oscilloscope, a feature well utilized in the subsequent sections. An overview of the ERTS is in the Fig. 6 and its design details are found in [20].

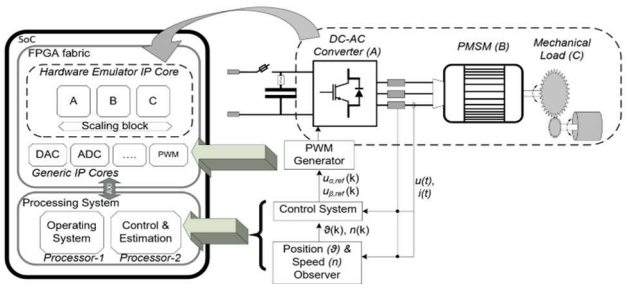

Fig. 6. Overview of the Embedded Real-Time Simulator used for IPMSM drive control-scheme validation

In the simulator, asymmetrical modulation with 3rd harmonic injection is applied. The switching and the digital controller sampling frequencies are 4 kHz and 8 kHz respectively. When the gain-scheduler is applied, r_s-estimation occurs in the speed envelop -21 to 21 rpm whereas ψ_m-estimation from |21| to |2100| rpm.

TABLE I. Simulation Data

	Symbol	***Value***	***Unit***
Nominal voltage	U_N	220	V
Nominal current	I_N	51	A
Nominal frequency	f_N	35	Hz
Pole pairs	p	1	-
Nominal speed	N_{rated}	2100	rpm
Initial Motor parameter vector	$[\psi_m\ x_d\ x_q\ r_s]^T$	$[0.66\ 0.4\ 1\ 0.009]^T$	pu
Gain-sequences in Hessian & L_{11} ,L_{12} computation	γ_0	6.25e-4	pu
Gain-sequences in L_{21} ,L_{22} computation	γ'_0	1.875e-5	pu

A. Perforamce of the Online Parameter Estimator

Firstly, the OPE-scheme is attempted to validate using the ERTS. To investigate the online adaption of the r_s-estimate following conditions have been applied: rotor speed = 0 pu; constant load torque = 0.5 pu; motor-r_s goes through a step change from 0.009 to 0.0072 pu.

Such experimentation resembles an identification run (or an ID-run) in an industrial drive to identify the stator resistance at the start-up of the machine. Fig. 7 presents the tracking performance where the adaptation completed within 5 seconds. Adaptation speed can be increased by increasing the γ'_0 at the expense of increased oscillations during the adaptation process. Similarly, the ψ_m-adaptation is tested with under the following conditions: rotor speed = 0.5 pu;

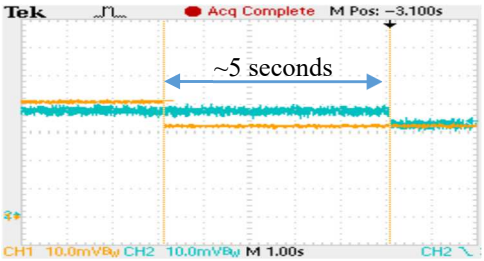

Fig.7. Online r_s adaptation at standstill. Yellow: motor resistance (pu), Blue: model resistance (pu)

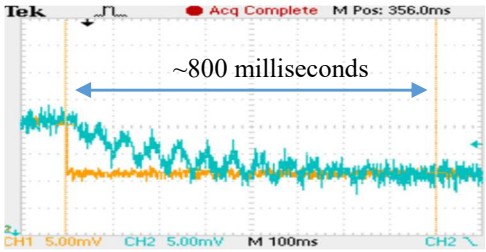

Fig. 8. Online ψ_m adaptation at 0.5 pu speed. Yellow: motor PM flux linkage (pu), Blue: model PM flux linkage (pu)

quadratic load torque; motor-ψ_m goes through a step change from 0.78 to 0.66 pu. The convergence is captured in the Fig. 8 which takes less than 1 second. Here, relatively faster convergence is achieved with a trade-off of relatively high oscillations in the tracking trajectory. In general, the adaption times with use of RPEM are in the range of a few seconds which is reasonable given the large thermal capacity of the temperature-sensitive parameters. The tracking performance can be anyway easily finetuned using the gain-sequences.

B. Experimentation of Sensorless Schemes

The AFO and the PUVI-based saliency tracking methods are investigated in this section while keeping the IPMSM parameters unchanged (thus the OPE is made redundant). Fig. 9 demonstrates the AFO performance when the speed-reference receives a step-change from 0.4 to -0.4 pu. The speed-reference, as seen in the figure, changes smoothly owing to a filtering process with a 100 ms time-constant. It is evident that the AFO is sufficiently robust to estimate the rotor position and speed when crossing the zero-speed. Fig. 10 shows how the AFO performs during persistent low speed operation (0.1 pu) which is reasonable.

The PUVI-based saliency-tracking method performance is as shown in the Fig. 11 when the speed reference varies from -0.01 pu to +0.01 pu.

C. Experimentation of Active Flux Observer Performance when the IPMSM Parameters Vary

Under this discussion, ψ_m , and r_s are varied in different speed regions to evaluate the AFO performance with and without the OPE. Firstly, the ψ_m -influence on the torque production (thus on the rotor -speed and -position) is investigated in the Fig. 12 and 13, where the first one with disabled OPE, the latter with the enabled OPE. In both cases, ψ_m is varied from 0.78 to 0.66 pu. The speed reference is 0.2 pu. The position error in the first case is 0.8 radians whereas when OPE is enabled, the same is reduced to -0.08 radians indicating a significant speed/torque control owing to the OPE. The same investigation is performed in relation to r_s. Here the speed reference is kept at 0.05 pu while the r_s is

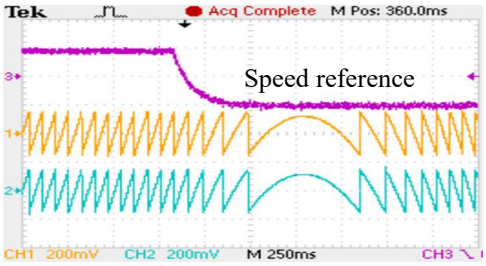

Fig. 9. Active Flux Observer performance when speed varies from 0.4 to -0.4 pu. Yellow: Actual rotor position (rad), Blue: Estimated rotor position (rad)

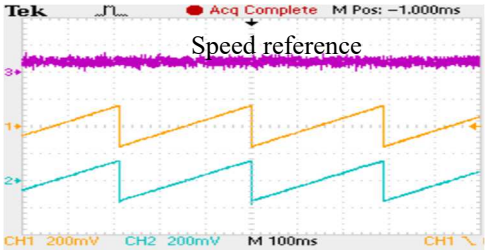

Fig.10. Active Flux Observer performance when persistent operation at 0.1 pu. Yellow: Actual rotor position (rad), Blue: Estimated rotor position (rad)

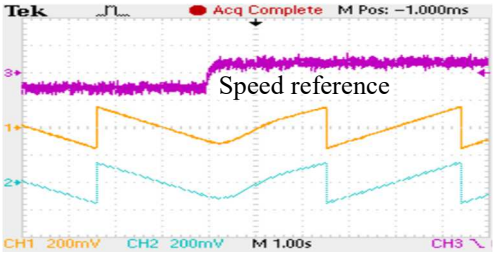

Fig. 11 7. Saliency tracking method performance when speed changes from -0.01 to +0.01 pu. Actual rotor position (rad), Blue: Estimated rotor position (rad)

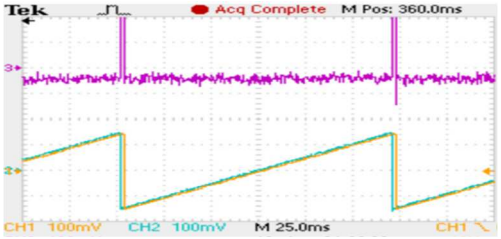

Fig. 12. AFO performance without OPE at 0.2 pu speed when ψ_m varies from 0.78 to 0.66. Yellow: Actual rotor position (rad), Blue Estimate rotor position (rad) Purple: Mean estimation error = -0.8 rad

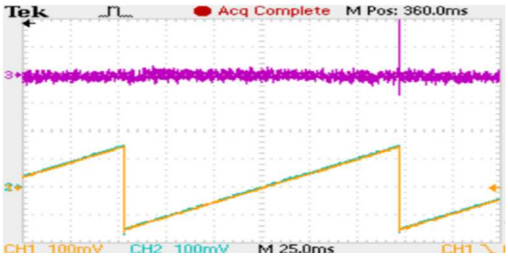

Fig.13. AFO performance with OPE at 0.2 pu speed when ψ_m varies from 0.78 to 0.66. Yellow: Actual rotor position (rad), Blue Estimate rotor position (rad), Purple: Estimation Error = -0.08 rad

varied from 0.009 to 0.0108 pu. When OPE is disabled, the mean position error is read to be -0.4 rad (Fig. 14) while the

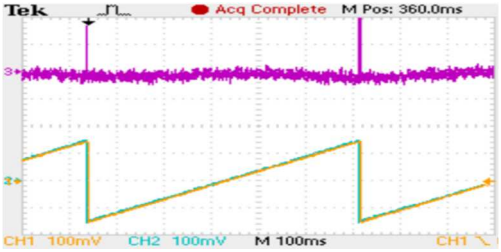

Fig. 14. AFO performance without OPE at 0.2 pu speed when ψ_m varies from 0.78 to 0.66. Yellow: Actual rotor position (rad), Blue Estimate rotor position (rad), Purple: Mean estimation error = -0.4 rad

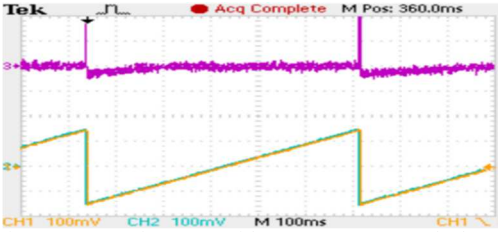

Fig.15. AFO performance with OPE at 0.2 pu speed when ψ_m varies from 0.78 to 0.66. Yellow: Actual rotor position (rad), Blue Estimate rotor position (rad), Purple: Mean estimation error = -0.13 rad

OPE is activated, the same reduces to -0.13 rad (Fig. 15) signifying a healthy improvement in the estimation accuracy thanks to the OPE.

V. CONCLUSION

This paper demonstrated the effective combination of a rather novel online parameter estimation scheme with high performance position-estimation methods to design a full speed range adaptive and sensorless IPMSM drive applicable for mission-critical applications under varying temperatures. The parameter-independence of the Square-wave Signal Injection based saliency tracking method is capitalized to circumvent the potential drawbacks of using a gain-scheduler around zero-speed. In the remaining speed regions, the estimation accuracy of the Active Flux Observer is improved by adapting the temperature-sensitive parameters online, thus the parameter-error effect on the full speed range is either minimized or eliminated. The powerful processors in the Xilinx System-on-Chip could accommodate the algorithm processing within the interrupt-cycle with ample time margins. Improving the Active Flux Observer with use of the saliency tracking method in the very low speed with the aim of tuning it for operation can be interesting further work.

REFERENCES

[1] J. Holtz, "Acquisition of position error and magnet polarity for sensorless control of PM synchronous machines," *IEEE Trans. Ind. Appl.*, vol. 44, no. 4, pp. 1172–1180, 2008.

[2] A. G. Jack, B. C. Mecrow, and J. A. Haylock, "A Comparative Study of Permanent Magnet and Switched Reluctance Motors for High-Performance Fault-Tolerant Applications," *IEEE Trans. Ind. Appl.*, vol. 32, no. 4, pp. 889–895, 1996.

[3] M. Schroedl, "Sensorless control of AC machines at low speed and standstill based on the `INFORM' method," *Conf. Rec. - IAS Annu. Meet. (IEEE Ind. Appl. Soc.*, vol. 1, pp. 270–277, 1996.

[4] S. Ovrebo and R. Nilsen, "New self sensing scheme based on INFORM, heterodyning and Luenberger observer," *IEMDC 2003 - IEEE Int. Electr. Mach. Drives Conf.*, vol. 3, pp. 1819–1825, 2003.

[5] P. L. Jansen and R. D. Lorenz, "Transducerless Position and Velocity Estimation in Induction and Salient AC Machines," *IEEE Trans. Ind. Appl.*, vol. 31, no. 2, pp. 240–247, 1995.

[6] M. J. Corley and R. D. Lorenz, "Rotor position and velocity estimation for a salient-pole permanent magnet synchronous machine at standstill and high speeds," *IEEE Trans. Ind. Appl.*, vol. 34, no. 4, pp. 784–789, 1998.

[7] Y. D. Yoon, S. K. Sul, S. Morimoto, and K. Ide, "High-bandwidth sensorless algorithm for AC machines based on square-wave-type voltage injection," *IEEE Trans. Ind. Appl.*, vol. 47, no. 3, pp. 1361–1370, 2011.

[8] S. Kim, J. I. Ha, and S. K. Sul, "PWM switching frequency signal injection sensorless method in IPMSM," *IEEE Trans. Ind. Appl.*, vol. 48, no. 5, pp. 1576–1587, 2012.

[9] R. Ni, D. Xu, F. Blaabjerg, K. Lu, G. Wang, and G. Zhang, "Square-Wave Voltage Injection Algorithm for PMSM Position Sensorless Control With High Robustness to Voltage Errors," *IEEE Trans. Power Electron.*, vol. 32, no. 7, pp. 5425–5437, 2017.

[10] A. Perera and R. Nilsen, "Gauss-Newton : A Prediction-Error-Gradient based Algorithm to Track PMSM Parameters Online," in *IEEE International Conference on Power Electronics, Drives and Energy Systems (PEDES)*, 2020, p. 8.

[11] A. Perera and R. Nilsen, "A Sensorless Control Method for IPMSM with an Open-Loop Predictor for Online Parameter Identification," in *23rd International Conference on Electrical Machines and Systems, ICEMS*, 2020, pp. 1983–1988.

[12] Y. Inoue, Y. Kawaguchi, S. Morimoto, and M. Sanada, "Performance improvement of sensorless IPMSM drives in a low-speed region using online parameter identification," *IEEE Trans. Ind. Appl.*, vol. 47, no. 2, pp. 798–804, 2011.

[13] A. Piippo, M. Hinkkanen, and J. Luomi, "Adaptation of motor parameters in sensorless PMSM drives," *IEEE Trans. Ind. Appl.*, vol. 45, no. 1, pp. 203–212, 2009.

[14] A. Perera and R. Nilsen, "A Framework and an Open-Loop Method to Identify PMSM Parameters Online," in *23rd International Conference on Electrical Machines and Systems, ICEMS*, 2020, pp. 1945–1950.

[15] S. Morimoto, M. Sanada, and Y. Takeda, "Mechanical sensorless drives of IPMSM with online parameter identification," *IEEE Trans. Ind. Appl.*, vol. 42, no. 5, pp. 1241–1248, 2006.

[16] S. C. Agarlita, I. Boldea, and F. Blaabjerg, "High-frequency-injection-assisted 'active-flux'-based sensorless vector control of reluctance synchronous motors, with experiments from zero speed," *IEEE Trans. Ind. Appl.*, vol. 48, no. 6, pp. 1931–1939, 2012.

[17] S. C. Yang and Y. L. Hsu, "Full Speed Region Sensorless Drive of Permanent-Magnet Machine Combining Saliency-Based and Back-EMF-Based Drive," *IEEE Trans. Ind. Electron.*, vol. 64, no. 2, pp. 1092–1101, 2017.

[18] F. Peng, Y. Yao, Z. Wang, Y. Huang, H. Yang, and B. Xie, "Position Estimation Method of IPMSM in Full Speed Range by Simplified Quadratic Optimization," *IEEE Access*, vol. 8, pp. 109964–109975, 2020.

[19] M. C. Paicu, I. Boldea, G.-D. Andreescu, and F. Blaabjerg, "Very low speed performance of active flux based sensorless control: interior permanent magnet synchronous motor vector control versus direct torque and flux control," *IET Electr. Power Appl.*, vol. 3, no. 6, p. 551, 2009.

[20] A. Perera, R. Nilsen, T. Haugan, and K. Ljøkelsøy, "A Design Method of an Embedded Real-Time Simulator for Electric Drives using Low-Cost System-on-Chip Platform," in *PCIM Europe digital days, In Press*, 2021.

[21] G. Wang, G. Zhang, and D. Xu, "Saliency-Tracking-Based Sensorless Control for PMSM Drives," in *Position Sensorless Control Techniques for Permanent Magnet Synchronous Machine Drives*, Singapore: Springer, Singapore, 2020, pp. 37–80.

[22] X. Jin, R. Ni, W. Chen, F. Blaabjerg, and D. Xu, "High-Frequency Voltage-Injection Methods and Observer Design for Initial Position Detection of Permanent Magnet Synchronous Machines," *IEEE Trans. Power Electron.*, vol. 33, no. 9, pp. 7971–7979, 2018.

[23] A. Perera and R. Nilsen, "A Recursive Prediction Error Method with Effective Use of Gradient-Functions to Adapt PMSM- Parameters Online," in *IEEE Industry Applications Society Annual Meeting*, 2020, pp. 2–6.